Applied Surface Science Advances 25 (2025) 100664

Contents lists available at ScienceDirect

Applied Surface Science Advances

journal homepage: www.sciencedirect.com/journal/applied-surface-science-advances

Full Length Article

Sodium cation exchanged zeolites for direct air capture of CO_2

Do Yeong Kim [a], Wo Bin Bae [a], Haehyun Min [a], Kyeong-Hun Ryu [a], Sungjoon Kweon [b], Linh Mai Tran [b], Young Jin Kim [c], Min Bum Park [b,*], Sung Bong Kang [a,d,*]

[a] School of Environment and Energy Engineering, Gwangju Institute of Science and Technology, Gwangju 61005, Republic of Korea
[b] Department of Energy and Chemical Engineering, Incheon National University, Incheon 22012, Republic of Korea
[c] Department of Environmental Engineering, Kyungpook National University, 80 Daehak-ro, Daegu 41566, Republic of Korea
[d] Research Center for Innovative Energy and Carbon Optimized Synthesis for Chemicals, Gwangju Institute of Science and Technology, Gwangju 61005, Republic of Korea

ARTICLE INFO

Keywords:
CO_2
Direct air capture
Zeolite
Na^+-exchange
Acid-basic site

ABSTRACT

Direct air capture technology requires investigating materials that can capture carbon dioxide inexpensively and efficiently, considering their performance under real atmospheric conditions. This study systematically investigated the CO_2 adsorption-desorption performance of the representative zeolites (ZSM-5, Beta, Mordenite and Y) in H- and Na-forms using various analytical methods, including in-situ Diffuse Reflectance Infrared Fourier Transform spectroscopy. Compared to the corresponding H-zeolites, the enhancement of CO_2 adsorption capacity by Na^+ ions was observed for all the structure-type zeolite adsorbents. The Na-ZSM-5 showed excellent performance in the direct air capture of CO_2 (DAC) due to its relatively smaller pore size and stronger acid-basic properties. The effective adsorption capacity of Na-ZSM-5 was pronounced at lower Si/Al ratios, making it the most efficient low-concentration CO_2 adsorbent. The low silica Na-ZSM-5 exhibited a durable adsorption-desorption capacity after multiple cycles, indicating its practical reusability. When applied to real atmospheric air conditions, this low silica Na-ZSM-5 effectively adsorbed CO_2 in the presence of oxygen and moisture, emphasizing its potential for a direct air capture adsorbent. This study provides insights into the properties of zeolites for CO_2 capture from air, highlighting their potential as effective DAC sorbents that can be produced on a large scale.

1. Introduction

Direct air capture (DAC) is a negative-emissions technology that captures CO_2 from the atmosphere, removing even the anthropogenic CO_2 already emitted. However, prevalent sorbent materials in current DAC applications face challenges like low adsorption capacity due to the low partial pressure of CO_2 in the air, stability issues and high energy requirements during regeneration [1]. To construct a feasible DAC system, efficient adsorbents are required with low energy penalties, cost-effectiveness, and high adsorption capacity.

Various solid sorbents, such as zeolites, metal-organic frameworks (MOFs), activated carbon, mesoporous silica, mesoporous alumina, metal oxides, covalent organic polymers, and amine-based materials, have been considered state-of-the-art technologies for atmospheric CO_2 capture [2–12]. Among them, zeolites have drawn significant interest in the context of CO_2 capture due to their highly ordered porous structure and small gas molecule size. Ideal materials for CO_2 capture require additional features, such as high chemical and thermal stability, accessible surface features, a large specific surface area, and a porous structure that can be modified on the surface through processes such as ion-exchange or impregnation, all of which zeolite can satisfy [13]. It has been well known that alkali or alkaline earth metal ions exchanged onto the extraframework of zeolites increase the electron density of framework oxygen, enabling high adsorption of Lewis acidic small molecules like CO_2 and NO_x [14]. Furthermore, the raw materials for zeolite synthesis can be sourced from waste materials or natural resources, from which the manufacturing cost can be significantly reduced [15]. Zeolites are widely available and can be synthesized in large quantities using low-cost processes, compared to other advanced materials [16]. As such, zeolite adsorbents have great potential to be cost-efficient candidates for DAC systems.

However, one of the significant challenges associated with zeolites is their performance degradation in the presence of water vapor (H_2O). This degradation has been the subject of extensive research, which has

* Corresponding authors.
E-mail addresses: mbpark@inu.ac.kr (M.B. Park), sbkang@gist.ac.kr (S.B. Kang).

https://doi.org/10.1016/j.apsadv.2024.100664
Received 26 June 2024; Received in revised form 4 November 2024; Accepted 17 November 2024
Available online 29 November 2024

focused on various strategies to mitigate the impact of moisture. These strategies include pretreatment techniques for water removal, using high silica zeolites to increase hydrophobicity, and operating zeolites at cryogenic temperatures to minimize water interference [17–19]. In addition to moisture, the structural and chemical properties of zeolites critically influence their CO_2 adsorption performance. Notably, CHA- and MOR-type zeolites have been found to exhibit superior CO_2 adsorption capacities due to their distinct pore structures, including 8-ring side pockets that serve as primary sites for CO_2 capture [20–22]. Furthermore, the efficiency of CO_2 adsorption is significantly affected by the charge-to-size ratio of metal cations within the zeolite framework, highlighting the importance of cation selection and its impact on the material's performance [23]. Despite this work, there remains a critical need to evaluate zeolite performance under more realistic conditions that include varying moisture levels and operational temperatures closer to ambient conditions. Such evaluations are essential to fully understand and optimize the practical efficacy of zeolites in DAC applications, ensuring that they perform effectively in real-environments [24].

To the best of our knowledge, surprisingly, few studies have been carried out into the adsorption of CO_2 over zeolites with a focus on DAC under real atmospheric air, corresponding to atmospheric pressure at room temperature. The concentration of CO_2 as an adsorption target is approximately 400 ppm, existing at an exceedingly low partial pressure. Besides, the atmosphere contains not only CO_2 but also substantial amounts of moisture and oxygen, much more than CO_2, unlike emissions from conventional industrial sources; thus, it is necessary to consider the effect of water and oxygen. Considering all this, we need to assess and analyze CO_2 adsorption performance under actual atmospheric circumstances, investigating the impact of other adsorbates in the air to improve the qualities of zeolite materials inside DAC systems. This knowledge should be instrumental for the perceptive development of zeolite characteristics that facilitate effective CO_2 capture under atmospheric air in the DAC system.

This study first aimed to evaluate the impact of zeolite structure and extraframework cation on CO_2 capture in low CO_2 concentrations simulating atmospheric levels. We characterized the CO_2 capture performance under real atmospheric air in the DAC system with respect to the zeolite structure. Furthermore, a diffuse reflectance infrared Fourier transform spectroscopy (DRIFTS) analysis was conducted to study the mechanism of the DAC system in detail.

2. Experimental section

2.1. Preparation of zeolite adsorbents

Commercial NH_4-ZSM-5 (Si/Al = 16) and H-Mordenite were purchased from Zeobuilder and Clariant, respectively. Also, NH_4-ZSM-5 zeolites with different Si/Al ratios (Si/Al = 11.5 (CBV2314), 25 (CBV5524G), 40 (CBV8014), and 140 (CBV28014)), NH_4-Beta (CP814E), and H-Y (CBV720) were obtained from Zeolyst. Before Na^+-exchange, all the H-form zeolites were converted to NH_4-form by refluxing three times in 1.0 M NH_4NO_3 aqueous solution (2 g solid per 25 mL solution) at 80 °C overnight. Then, all the NH_4-form zeolites were exchanged with 0.8 M NaCl aqueous solution at 80 °C for 1 h according to the similar procedure given above. The resulting solutions were dried at 80 °C using a rotary evaporator and washed several times with a centrifuge. Finally, the Na-form zeolites were obtained by calcination at 550 °C for 4 h. In addition, the H-form zeolites were prepared by simple calcination of the NH_4-forms at 550 °C for 4 h.

2.2. DAC performance tests

The CO_2 adsorption-desorption tests were conducted under atmospheric pressure in a flow-type quartz tube reactor loaded with around 0.08–0.10 g of zeolite powder. Before each adsorption test, the zeolite adsorbent sample in a tube was preheated from 25 to 450 °C at a ramp rate of 10 °C min^{-1} in He flow (100 mL min^{-1}) and then maintained at 450 °C for 2 h. After cooling down to 25 °C using liquefied N_2 under He flow, a feed gas mixture with 100 mL min^{-1} containing 400 ppm CO_2 in He balance was passed to the loaded sample at 25 °C for 2 h as an adsorption test. As a result, the breakthrough curve in CO_2 adsorption was obtained. After the full saturation with CO_2, two desorption behaviors were monitored, one for the desorption of physisorbed CO_2 at 25 °C for 1 h and the other for the desorption of chemisorbed CO_2 (temperature programmed desorption of CO_2, CO_2-TPD) with increasing temperature to 300 °C (5 °C min^{-1}). The desorption experiments were performed using the He flow. The gas hourly space velocity (GHSV) of this CO_2 breakthrough curve system was maintained at 125,000 h^{-1}, corresponding to 100 mL min^{-1} of the total flow rate. The outlet CO_2 gas concentration during the CO_2 adsorption and desorption test was continuously monitored using BELCAT II (MicrotacBEL. Corp.) equipped with a thermal conductivity detector (TCD). Each adsorption-desorption capacity of CO_2 was calculated from the TCD data gap between the blank and the sample. In addition, to evaluate the durability of the prepared zeolite adsorbent, the CO_2 adsorption-desorption cycling tests were repeated 20 times under the identical conditions mentioned above. The pretreatment at 450 °C for 1 h was conducted only for the first cycle experiment, after which the adsorption experiments were performed directly following desorption without an activation process between each cyclic test.

The calcined powder zeolite without any binder was pressed using a pelletizer (EPQ-1 Manual Pellet Press, Orbit Tech.), which pressed the powder sample at 200 bar for 10 min and then sieved into 30–40 mesh size to make pellet forms of powder zeolites (Fig. S1). The pelletized sample was loaded into a quartz tube and tested in a packed-bed reactor for DAC performance at 27 °C under three parametric feed compositions: (1) 530 ppm CO_2 in N_2 balance, (2) 530 ppm CO_2 with 21 % O_2 in N_2 balance, and (3) atmospheric air. The real atmospheric air in urban Gwangju, Korea was fed into the reactor using an air compressor equipped with a mass controller (Jiangsu Hehui Power Tools Co., Ltd.), confirming that the standard concentration of the outdoor CO_2 is ~530 ppm. The CO_2 concentration in the dry condition was determined by the actual atmospheric CO_2 concentration of 530 ppm. The gas hourly space velocity (GHSV) of this CO_2 capture system was maintained at 100,000 h^{-1} ,which corresponds to 200 mL min^{-1} of the total flow rate. The concentration of CO_2 was measured using an in-situ Fourier-transform infrared spectrometer (FTIR, PerkinElmer Spectrum Two) equipped with a gas cell (PIKE Technologies, path length: 10 m). Before each adsorption test, the zeolite sample was pretreated using the same method as mentioned above. The DAC performances were tested at 27 °C, maintaining the room temperature of the reactor in the laboratory. The CO_2 adsorption capacity was calculated by integrating the breakthrough curve area of CO_2. The desorption tests were performed by purging with N_2 flow at 27 °C for 30 min, and then the temperature was increased from 27 to 450 °C at a ramping rate of 5 °C min^{-1}.

2.3. Characterization of zeolite adsorbents

The specific surface area of zeolites was analyzed according to the Brunauer–Emmett–Teller (BET) method applied to their N_2 adsorption isotherms at 77 K with BELSORP-mini-X (MicrotacBEL. Corp.) surface analyzer. The elemental analysis was conducted using an inductively coupled plasma optical emission spectrometer (ICP-OES) on a Thermo Scientific iCAP 7400 ICP-OES DUO instrument. The acidic properties of the solid samples were determined by NH_3-TPD connected to a BELCAT II (MicrotacBEL. Corp.) equipped with a TCD detector. The NH_3-TPD was carried out as follows: (a) Pretreatment at 450 °C for 2 h in a flow of pure He (50 mL min^{-1}), (b) cooling down to 25 °C and consecutive NH_3 adsorption with 3 % NH_3/He (50 mL min^{-1}) for 1 h at the same temperature, (c) desorption of physisorbed NH_3 with He flow (50 mL min^{-1}) for 1 h, and (d) NH_3-TPD with the same He flow from 25 to 600 °C (10 °C min^{-1}).

To distinguish the acidic properties of Brønsted and Lewis acid sites, the pyridine-adsorption IR (py-IR) spectra were acquired on a Shimadzu IRTracer-100 FT-IR spectrometer. A self-supporting zeolite wafer of approximately 20 mg with a 1.3 cm diameter was prepared and placed inside a custom-built IR cell. Subsequently, the samples were pretreated at 450 °C for 2 h under a He flow (30 mL min^{-1}). Thereafter, the temperature of the sample was naturally down to 100 °C, saturated with a pyridine-loaded flow of dry He (20 mL min^{-1}) for 10 min, and subsequently flushed with excess He flow (30 mL min^{-1}) at the same temperature for 30 min to remove the physisorbed pyridine. After desorption at 100 °C, the concentrations of Brønsted and Lewis acid sites were determined at different temperatures (100–450 °C) from the intensities of the IR bands at approximately 1550 and 1450 cm^{-1}, respectively, using the equations by Emeis [25].

To identify the CO_2 adsorption forms on the surface of zeolite adsorbent, the surface-IR study was conducted with in-situ DRIFTS spectrometer on the NICOLET iS50 FT-IR (Thermo Fisher Scientific) equipped with a MCT detector and DRIFTS reaction cell (DiffusIR™, PIKE Technologies, with a ZnSe window, heating cartridge, and 10 sec of scanning time). Before each measurement, a zeolite powder sample was purged by flowing pure N_2 at 450 °C for 2 h and cooled down to room temperature. The spectra of the sample were collected at 25 °C during CO_2 adsorption and then at 25, 70, 150 and 250 °C in purging with pure N_2. The IR spectra were collected with the following three conditions: (1) only CO_2 in N_2 balance, (2) CO_2 with 21 % O_2 in N_2 balance, and (3) atmospheric air.

3. Results and discussion

3.1. CO_2 sorption performance of Na-zeolites with respect to framework type

When evaluating DAC performance, it is particularly important to consider the impact of moisture, especially in the case of zeolites. Previous studies have shown that the presence of water vapor has been shown to significantly reduce CO_2 adsorption on Na-zeolites with low Si/Al ratios (Si/Al ratio ~6.5) at low CO_2 partial pressures, especially [26]. To minimize this effect, the application of hydrophobic zeolites with a higher Si/Al ratio could be considered. While this choice reduces the water effect, it does have limitations in low-concentration CO_2 applications [27]. Accordingly, we intently selected a Si/Al ratio that is neither too high (< 20) nor too low (> 10), aiming to reduce the impact of water vapor on CO_2 adsorption while ensuring sufficient CO_2 adsorption performance even at low CO_2 concentrations. Considering this, we employed four representative zeolites with different framework types (MFI, MOR, Beta and FAU) within similar Si/Al ratios (12.5–20) to compare their CO_2 sorption properties according to the zeolite structural features.

Their basic structural and physicochemical properties are summarized in Table 1. Na-zeolites with different frameworks were synthesized successfully and it can be seen that their peak positions were similar to H-form zeolites with no other impurity phase (Fig. S2). This suggests that the structure was well maintained without any change after Na^+ was exchanged. The resulting elemental contents of ion-exchanged Na^+ ranged in a narrow level of 1.3–1.8 wt.%. As expected, Na-Beta and Na-Mordenite, which have the lowest (12.5) and highest (20) Si/Al ratio, resulted in the highest (1.8 wt.%) and lowest (1.3 wt.%) Na contents, respectively. As shown in Table 1, the Na/Al ratio is observed to be less than 1. The degree of ion exchange is often less than 100 %, which results in a Na/Al ratio of less than 1. This incomplete ion exchange can occur due to various factors, including the accessibility of the cation exchange sites and the specific conditions used during the ion exchange process. Moreover, some aluminum atoms can migrate from the tetrahedral framework during the calcination process, forming extraframework aluminum species that occupy octahedral sites, resulting in a Na/Al ratio lower than 1 [28].

Table 1
Structural features and physicochemical properties of H- and Na-zeolites.

Zeolite	IZA code	Crystal structure symmetry	Pore topology	Pore size (Å)	Chemical composition			BET surface area ($m^2 g^{-1}$)[d]			Micropore volumes ($cm^3 g^{-1}$)[d]
					Si/Al[a]	Na (wt.%)[b]	Na/Al[b]	Total	External	Micropore	
H-ZSM-5	MFI	Orthorhombic	3D, 10-ring	5.1 × 5.5, 5.3 × 5.6	16	-[c]	-[c]	477	18	459	0.30
Na-ZSM-5						1.8	0.66	395	15	380	0.16
H-Mordenite	MOR	Orthorhombic	3D, 12 and 8-rings	6.5 × 7.0, 2.6 × 5.7	20	-[c]	-[c]	454	30	424	0.18
Na-Mordenite						1.3	0.52	466	27	439	0.21
H-Beta	Beta	Tetragonal	3D, 12-ring	6.5 × 6.7, 5.6 × 5.6	12.5	-[c]	-[c]	644	182	462	0.18
Na-Beta						1.8	0.54	675	189	486	0.21
H-Y	FAU	Cubic	3D, 12-ring	7.4 × 7.4	15	-[c]	-[c]	825	96	729	0.25
Na-Y						0.59	0.59	832	100	732	0.26

[a] Provided from the commercial products.
[b] Determined by ICP elemental analysis.
[c] Not determined.
[d] Calculated from N_2 sorption isotherm data, applying the BET and *t*-plot methods.

In addition, all the prepared H- and Na-zeolites exhibited enough micropore volumes higher than 0.16 $cm^3\ g^{-1}$ to be confirmed that their micropore structures were still maintained even after the several treatments of each commercial zeolite. However, when Na^+ ion was exchanged in the ZSM-5, the micropore volume of Na-ZSM-5 was reduced compared to its H-form. Results clearly point to the incorporation of the cation species into the micropore space of ZSM-5, which is reflected by the lower pore volume from 0.30 to 0.16 $cm^3\ g^{-1}$ within the micropore [29]. The Mordenite has not only large pores of 12 rings but also small pores such as 8 rings, which makes it effective for CO_2 capture like ZSM-5. Fu et al. demonstrated that Na cations present in the 8MR side pockets can act as the main adsorption sites through a confinement effect, achieving CO_2 capacities of up to ~11.5 mmol g^{-1} [22]. However, the Mordenite used in this study had a high Si/Al above 10, which made Na cations less likely to occupy the 8MR side pockets, resulting in a reduced sealing effect and consequently a relatively low CO_2 adsorption performance.

Fig. 1 shows the CO_2 adsorption breakthrough curves obtained at 25 °C with a feed stream consisting of 400 ppm CO_2 in He balance and the CO_2-TPD profiles for all the H- and Na-zeolite adsorbents listed in Table 1. For H-form zeolites (Fig. 1a), their adsorption breakthrough curves of CO_2 were marginal, almost similar to the blank profile, which indicates that CO_2 molecules are scarcely adsorbed on the bare H-zeolites. Of course, all the H-zeolites also exhibited a negligible amount of desorbed CO_2 (Fig. 1b). While the zeolite framework oxygen has weak basicity and tends to become stronger at lower Si/Al ratios [30], even the H-Beta with the lowest Si/Al among the zeolites prepared in this study did not show any distinct CO_2 adsorption. CO_2 adsorption is attributed to the combined stronger chemisorption and relatively weaker physisorption, which can be caused by the natural zeolite framework property and/or the artificially induced adsorption sites like extraframework elements. It has been reported that the Na^+ ions interact with the zeolite framework oxygen, providing basicity that facilitates the adsorption of Lewis acidic CO_2 [31]. Furthermore, the enhanced CO_2 adsorption capacity may arise from ion-quadrupole interactions between Na^+ and CO_2 [32]. Even if there is just sufficient space for CO_2 molecules (e.g., super-cage inside zeolite Y), a strong primary adsorption site to attract CO_2 is required, especially in the DAC system.

Fig. 1c presents that the Na^+ ions exchanged in zeolites enable an apparent CO_2 trapping, which is sensitive to the structure type. The

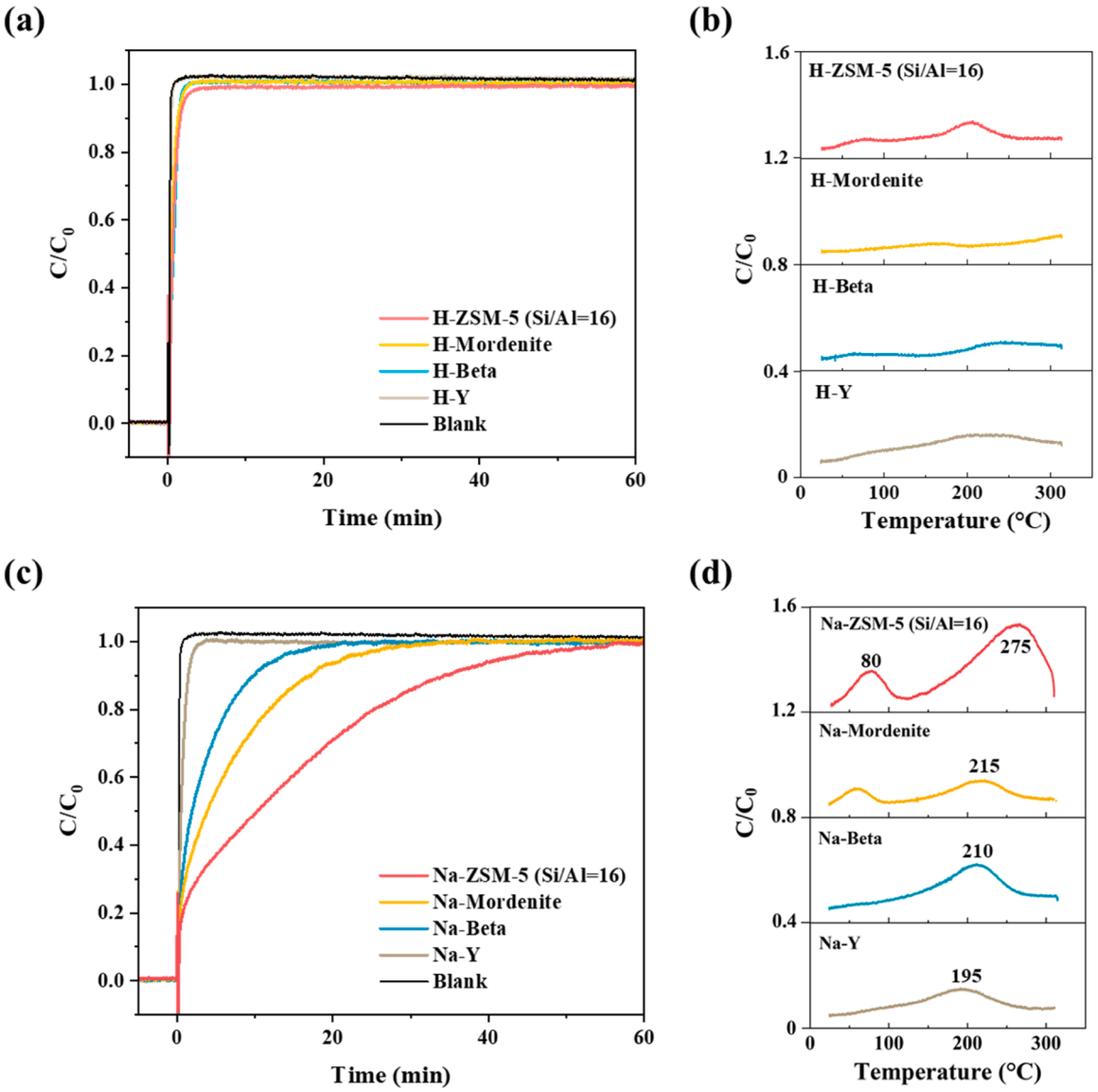

Fig. 1. CO_2 adsorption-desorption performance of zeolite adsorbents with different structures and cation forms. Adsorption condition: 400 ppm CO_2 in balance N_2 at 25 °C, GHSV of 125,000 hr^{-1} and total flow rate of 100 mL•min^{-1}. CO_2 adsorption breakthrough curves for (a) H-form and (c) Na-form zeolites under, and (b and d) their CO_2-TPD profiles. Here, the Si/Al ratio of ZSM-5 is 16. For comparison, the adsorption experiment in the absence of adsorbent (blank) was also conducted.

results are also summarized in Table 2. Na-ZSM-5 showed the highest CO_2 adsorption capacity (0.37 mmol g^{-1}) with CO_2 adsorption for 1 h while other zeolites were saturated with adsorbed CO_2 in a short time. The adsorption amount decreased as the zeolite pore size increased, where the larger the pore zeolites, the faster the breakthrough kinetics with its saturation. Although the Na-Y showed the lowest CO_2 adsorption capacity among the Na-zeolites, it showed a distinct CO_2 adsorption compared to the bare H-Y. This indicates the primary effect of Na^+ on CO_2 adsorption rather than the bare zeolite framework. Even though the Na contents are almost similar, the smaller the pore size, the greater the CO_2 adsorption, indicating that the CO_2 capture was induced through the increased affinity between Na^+ adsorption sites and CO_2 due to the smaller pore size. Unlike other zeolites, the Na-ZSM-5 zeolite showed a decrease in BET surface area from 477 to 395 m^2 g^{-1} after Na^+ ion exchange, with a particularly significant reduction in micropore surface area. The Na^+ ions can occupy narrower spaces or exist at the intersections between the straight and sinusoidal channels within MFI structures, which could lead to a stronger affinity for CO_2 compared to other zeolite structures [33]. However, it should be noticed that not all the Na^+ in zeolites can be accessed by the guest molecules and in this regard, the number of CO_2 molecules adsorbed per Na^+ ion was observed to be less than 50 %. When comparing the number of CO_2 molecules adsorbed per single Na, those were calculated to be about 0.41 and 0.14 CO_2/Na for Na-ZSM-5 and Na-Y, respectively (Table 2). To further investigate the effect of the structural properties of each zeolite on CO_2 adsorption, the initial CO_2 adsorption behavior was compared. The initial CO_2 adsorption behavior of H-form zeolites also showed that little CO_2 adsorption occurred, especially for Y zeolite, which did not adsorb CO_2 (Fig. S3a). It seems that Y zeolite not only has a larger pore size than other zeolites but also has a super cage, which makes it more difficult to interact with small molecules of CO_2 (3.3 Å) due to the low affinity of CO_2. The initial CO_2 adsorption behavior of Na-zeolites is also consistent with the previous results: the smaller the pore size, the more CO_2 is adsorbed (Fig. S3b). This suggests that the zeolite structure exerts a secondary effect once the CO_2 adsorption is induced by Na^+.

The desorption experiments were also conducted for the four Na-zeolites right after their CO_2 adsorption. The continuous desorption profiles of physisorbed CO_2 were obtained at the same temperature of 25 °C for 1 h by purging the inert gas, and the CO_2-TPD profiles are illustrated in Figs. S4 and 1d, respectively. While the amount of physisorption increased in the order of the total amount of adsorption (i.e., Na-ZSM-5 > Na-Mordenite > Na-Beta > Na-Y), the chemisorption did not follow the trend (Table 2). The Na-Mordenite with the lowest Na content due to the highest Si/Al resulted in the lowest amount of chemisorption, again demonstrating that CO_2 molecules were adsorbed by Na^+ ions as a primary effect. In addition, as the pore size increased, that is, as the total adsorption amount of CO_2 decreased, the proportion of chemisorption was higher than that of physisorption among the total adsorption. For example, the relative physisorption/chemisorption ratio of Na-ZSM-5 was 0.18/(0.02 + 0.11) ~ 1.4, but that of Na-Y was only 0.40. This indicates that more physisorption is possible on the strong adsorption sites generated by the stronger affinity for CO_2 ions due to the effect of small pore size. These results are consistent with the previous findings showing a strong correlation between pore size and CO_2 adsorption performance, suggesting that small pore size plays a crucial role in the physisorption of CO_2 at low concentrations [34,35].

Furthermore, it is interesting to note here that Na-ZSM-5 and Na-Mordenite showed two resolved CO_2-TPD peaks, whereas Na-Beta and Na-Y showed a single broad band (Fig. 1d). Comparing the highest peak temperatures of Na-zeolites appeared on the higher temperature region, the smaller the pore size (Na-ZSM-5 < Na-Mordenite < Na-Beta < Na-Y), the higher the peak temperature (275 > 215 > 210 > 195 °C), i.e., the stronger chemisorption. This trend is consistent with the discussion for the adsorption amount described above. In particular, the unique medium-pore zeolite studied here, Na-ZSM-5 showed the strongest CO_2 chemisorption feature at around 275 °C, which is probably due to a unique adsorption mechanism different from the others. Another desorption peak appeared below 100 °C in Na-ZSM-5 and Na-Mordenite may be the result of relatively strongly physisorbed and/or weakly chemisorbed CO_2. MFI and MOR have 12 and 4 crystallographically different tetrahedral sites, respectively, and aluminum atoms are randomly distributed among them if there are no special synthetic treatments [36]. Therefore, structurally diverse Na^+ coordination environments are possible, and the sorption strength of CO_2 can vary accordingly [37]. It is worth noting that further screening of other alkali or alkaline earth metal ions over ZSM-5 for the DAC performance is now underway to confirm the effect of metal cations (i.e., Mg, K, Ca and Ba); we confirm that the Na^+ exchanged onto ZSM-5 is one of the best formulations compared to other cation exchanged (Data not shown).

3.2. CO_2 adsorption of Na-ZSM-5 with different Si/Al ratios

We examined the strong adsorption sites induced by Na^+, which could actively trap CO_2 molecules in atmospheric environments with a low level of CO_2 at room temperature. The adjacent Na^+ ions inside the small pores of zeolite significantly affect the maximum adsorption amount. To better understand the effect of Na^+ on the low concentration CO_2 capture, a series of ZSM-5 zeolites varying Si/Al ratios from 11.5 to 140 was compared as shown in Fig. 2 and Table 3. Obviously, as the Si/Al ratio increased, the content of ion-exchanged Na^+ decreased exponentially from 1.0 to 0.1 mmol g^{-1} (Fig. 2a). As the Na content decreased, the BET surface area gradually increased (Table 3).

Fig. 2b shows the adsorption breakthrough curves for the five Na-ZSM-5 zeolites with different Si/Al ratios. The CO_2 adsorption capacity was improved by a lowered Si/Al ratio, while the bare H-ZSM-5 zeolites exhibited a negligible CO_2 capturing performance regardless of the Si/Al ratio (Fig. S5). This again confirms the crucial role of Na sites in the DAC activity. Additionally, when comparing the adsorption behavior across different Si/Al ratios (Fig. S6), we observed that zeolites with low

Table 2
CO_2 adsorption-desorption capacities over Na-zeolites.

Zeolite	CO_2 adsorption[a]		CO_2 desorption[b]	
	Adsorbed (mmol g^{-1})[d]	CO_2/Na (mol.%)	Physisorbed (mmol g^{-1})[e]	Chemisorbed (mmol g^{-1})[f]
Na-ZSM-5[c]	0.37	41.0	0.18	0.02, 0.11
Na-Mordenite	0.18	27.3	0.10	0.01, 0.03
Na-Beta	0.14	18.0	0.07	0.08
Na-Y	0.08	14.1	0.02	0.05

[a] Adsorption condition: 400 ppm CO_2 in balance N_2 at 25 °C, GHSV of 125,000 hr^{-1} and total flow rate of 100 mL•min^{-1}.
[b] Desorption condition: The temperature is maintained at 25 °C for 1 h followed by an increase to 300 °C under He flow.
[c] Si/Al = 16.
[d] Calculated from the CO_2 adsorption breakthrough curves shown in Fig. 1c.
[e] Calculated from the CO_2 desorption profiles shown in Fig. S4.
[f] Calculated from the CO_2-TPD profiles shown in Fig. 1d.

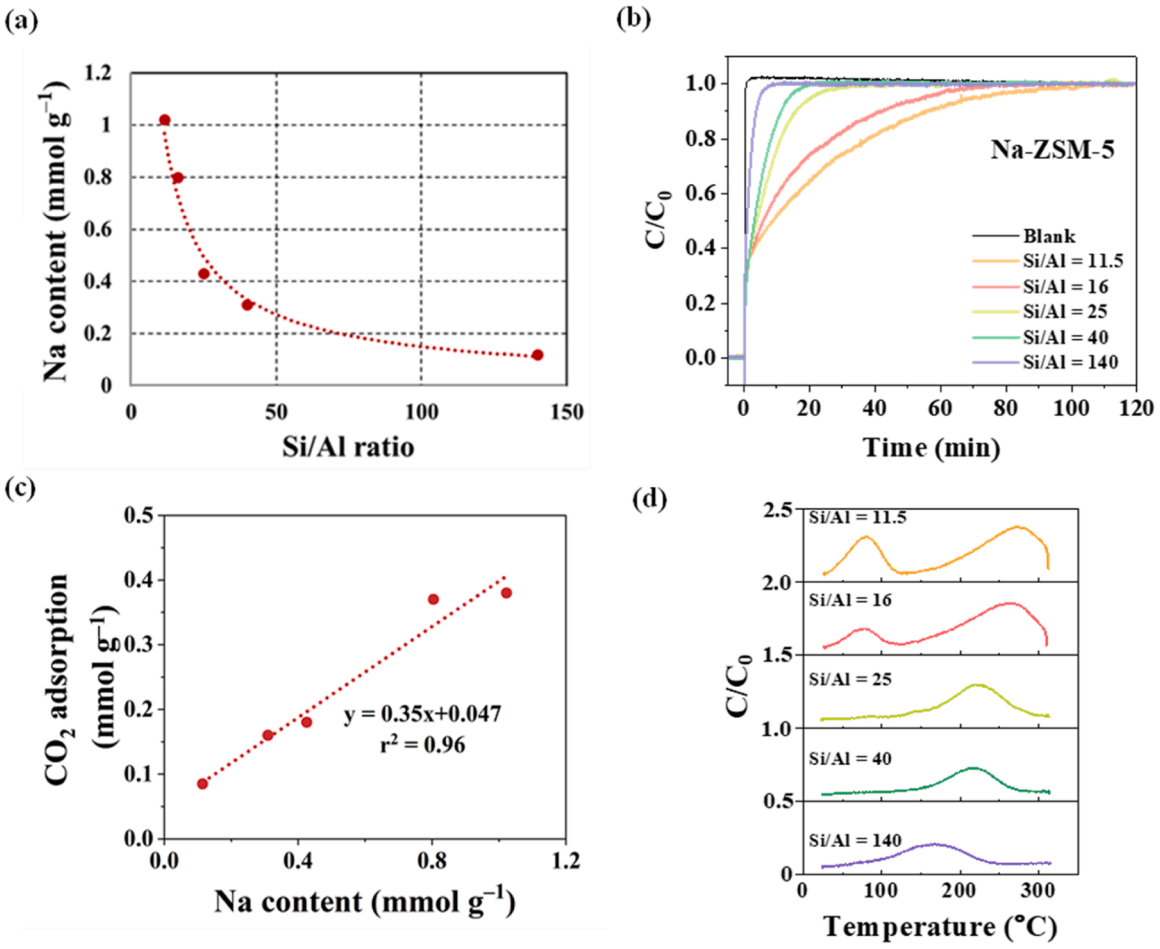

Fig. 2. CO_2 adsorption-desorption performance of Na-ZSM-5 zeolites with different Si/Al ratios. (a) Variation curves of Na content as a function of Si/Al ratio, (b) CO_2 adsorption breakthrough curves, (c) variation curves of CO_2 adsorption capacity as a function of Na content, and (d) CO_2-TPD profiles.

Table 3
Physicochemical properties and CO_2 adsorption-desorption capacities of Na-ZSM-5 zeolites with different Si/Al ratios.

Si/Al[a]	Na (wt.%)[b]	BET surface area (m^2 g^{-1})[c]			CO_2 adsorption	CO_2 desorption	
		Total	External	Micropore	Adsorbed (mmol g^{-1})[d]	Physisorbed (mmol g^{-1})[e]	Chemisorbed (mmol g^{-1})[f]
11.5	2.4	382	21	361	0.38	0.20	0.04, 0.11
16	1.8	395	15	380	0.37	0.18	0.02, 0.11
25	1.0	429	30	399	0.18	0.10	0.08
40	0.7	473	55	418	0.16	0.10	0.07
140	0.3	496	39	457	0.085	0.02	0.07

[a] Provided from the commercial products.
[b] Determined by ICP elemental analysis.
[c] Calculated from N_2 sorption isotherm data, applying the BET and *t*-plot methods.
[d] Calculated from the CO_2 adsorption breakthrough curves shown in Fig. 2b.
[e] Calculated from the CO_2 desorption profiles shown in Fig. S7.
[f] Calculated from the CO_2-TPD profiles shown in Fig. 2d.

Si/Al ratios (11.5 and 16) exhibited slower initial adsorption speeds compared to those with medium Si/Al ratios (25 and 40). This is due to the increased number of Na cations in zeolites with lower Si/Al ratios, which shield the micropore windows, making it more difficult for CO_2 to diffuse into the pores. While the Na-ZSM-5 with the highest Si/Al = 140 showed an adsorption breakthrough curve similar to that of Na-Y discussed above, the Na-ZSM-5 with the lowest Si/Al = 11.5 showed more improved CO_2 adsorption than the Na-ZSM-5 with Si/Al = 16 discussed previously. Even the Na-ZSM-5 containing the highest Na content continued adsorption for over 100 min under identical adsorption conditions. An interesting observation is the linear sensitivity in the CO_2 adsorption capacity to the Na content (Fig. 2c), demonstrating a controllable DAC performance by the cation content in zeolites.

Fig. 2d shows the CO_2-TPD profiles, while the physical desorption profiles at room temperature are compared in Fig. S7. When Na-ZSM-5 was divided into low (11.5 and 16), medium (25 and 40) and high (140) according to the Si/Al ratio in the macroscopic point, the proportion of physisorption was higher than that of chemisorption as the Na content increased. In particular, the relative physisorption/chemisorption ratio of Na-ZSM-5 with Si/Al = 140 was 0.02/0.07 ~ 0.29 (Table 3), similar to that of Na-Y (0.40). Notably, similar to the previous discussion of Na-zeolites with different structures but similar Na content, the proportion

of physisorption was higher than chemisorption as the Na content increased. However, in more detail, the Na-ZSM-5 adsorbents with Si/Al = 11.5 and 16 showed almost identical physical desorption tendency and the physisorption amount, but the former exhibited a higher amount of CO_2 chemisorption than the latter when comparing their CO_2-TPD profiles, especially in the low temperature region. This is likely due to the saturation of the physisorption sites created by the ion-exchange of Na in Na-ZSM-5 (Si/Al = 16), so Na-ZSM-5 (Si/Al = 11.5) has increased chemisorption sites instead of physisorption. This suggests that CO_2 physisorption sites as Na cations on ZSM-5 are formed first, followed by weak CO_2 chemisorption sites in the low Si/Al ratio region. Similarly, the Na-ZSM-5 with Si/Al = 25 and 40 also showed a similar trend in the medium Si/Al ratio region. This means that these Na-ZSM-5 adsorbents operate by a similar mechanism in adsorption and desorption. Furthermore, the Na-ZSM-5 with Si/Al = 11.5 and 16, which have higher Na contents and therefore more physisorption, showed the two resolved CO_2-TPD peaks, while the other three Na-ZSM-5 zeolites with lower Na contents exhibited only one broad band. The highest peak temperatures also shifted to high temperature regions gradually as the Na content increased. Taken together, the lower framework Si/Al ratio indicates that more Na^+ ions are available for CO_2 adsorption by creating stronger chemisorption sites as well as physisorption sites. These results once again strongly support that the Na^+ acts as a primary adsorption site for the low concentration CO_2 adsorption.

3.3. Surface characterization of CO_2 adsorption with respect to zeolite

To more precisely monitor the adsorption-desorption behavior of CO_2 molecule on Na-zeolite, the in-situ DRIFTS technique was used over the four zeolites with different framework types (i.e., MFI, MOR, Beta, and FAU listed in Table 1). The IR spectra were obtained after exposure to the CO_2/N_2 flow at 25 °C for 30 min in Na-zeolites (Fig. 3a), and the spectra were continuously monitored in N_2 flow at a temperature range of 25 to 250 °C in the Na-ZSM-5 (Fig. 3b). Unlike the IR spectra of the H-zeolites which had one strong band at around 2346 cm^{-1} assignable as hydrogen-bonded or physically adsorbed CO_2 (Fig. S8) [38], the corresponding Na-zeolites exhibited several characteristic peaks representatively appeared at around 1639, 2291, 2341, 2347, 2355, 2371, 2410 cm^{-1}, etc. (Fig. 3a). The Na-Y with the lowest CO_2 adsorption capacity showed one strong IR peak similar to H-zeolites, but its wavenumber (2355 cm^{-1}) was higher than those of H-zeolites. This is a typical characteristic peak for the O=C=O vibrational mode (ν_3) linearly adsorbed on the basic site caused by Na^+ (Scheme 1b) [39,40]. Two additional shoulders observed at 2291 and 2410 cm^{-1} can be assigned to ν_3 mode of O=^{13}C=O and combined mode ($\nu_3 + \nu_{is}$) of O=C=O adsorbed on Na^+, respectively, where ν_{is} represents the intermolecular cation-oxygen stretching of the $Na^+\cdots$O=C=O adduct. This simple and representative CO_2 adsorption behavior was observed as a similar amount of Na^+ ions were distributed sparsely within the large pores of Na-Y.

Compared to Na-Y, several characteristic peaks appeared over smaller pore zeolites. Among these, the relatively low intensity peaks were presented at 2341 and 2371 cm^{-1}. The experimentally found value for CO_2 is ν_3 = 2341 cm^{-1}, which is 8 cm^{-1} smaller than the corresponding value for free CO_2 (ν_3 = 2349 cm^{-1}). However, it should be noticed that CO_2 adsorbed on a pure silica zeolite shows ν_3 = 2341 cm^{-1}, hence the experimentally found value for CO_2 in Na-zeolite is blue-shifted [41]. Another relatively low intensity peak at 2371 cm^{-1} can be assigned as the CO_2 adsorption on extraframework Al^{3+} ions [39]. Instead of the strong peak at 2355 cm^{-1} observed in Na-Y, the other three Na-zeolites showed the strong characteristic peak at 2347 cm^{-1}, and this became more prominent in Na-ZSM-5 where the pore size

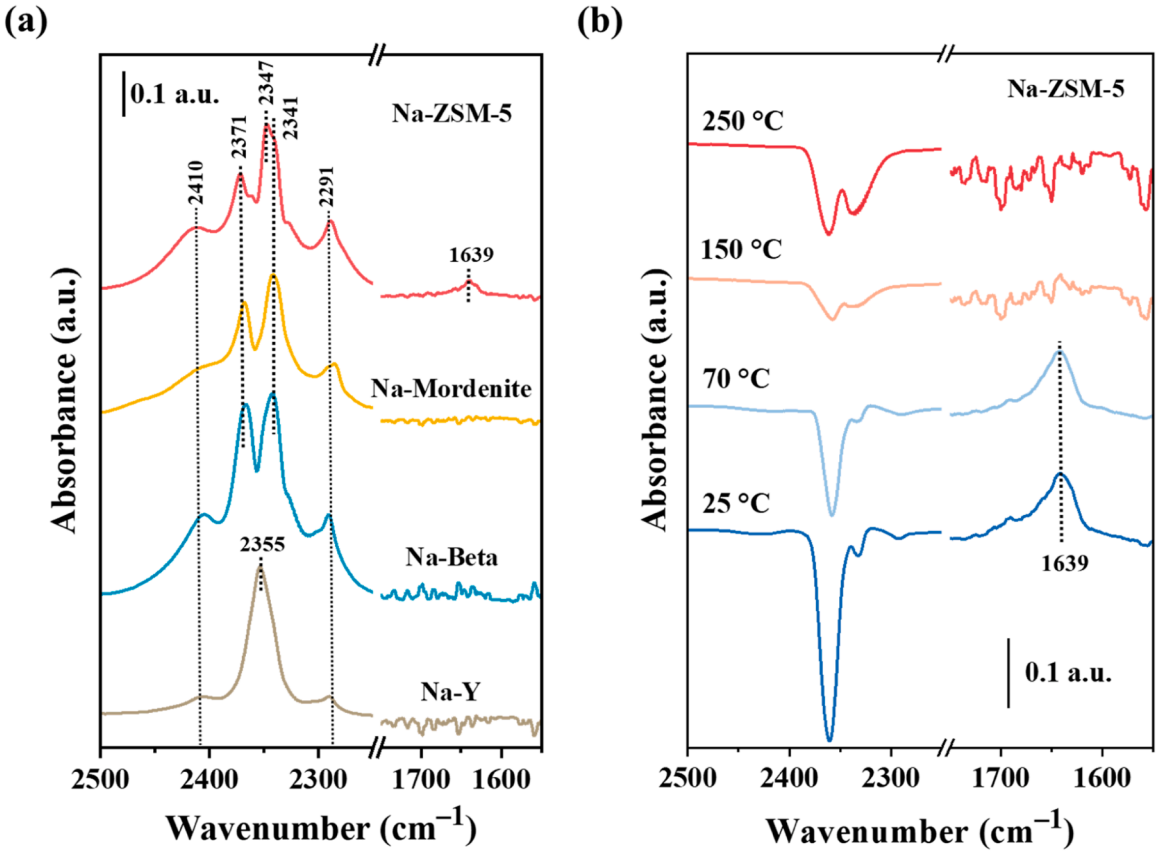

Fig. 3. Characterization of adsorbed species in CO_2 adsorption-desorption over Na-zeolites. (a) DRIFT spectra measured under the flow of CO_2 with N_2 balance at 25 °C and (b) DRIFT spectra measured during CO_2 desorption in N_2 flow from 25 to 250 °C on Na-ZSM-5. Here, the Si/Al ratio of Na-ZSM-5 is 16.

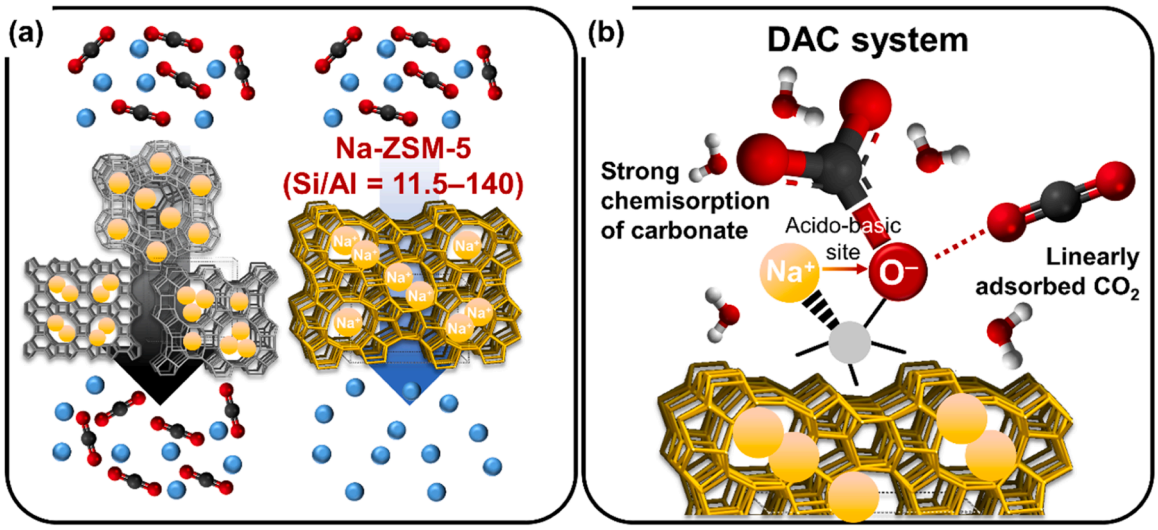

Scheme 1. (a) Comparison of CO_2 capture performance on various zeolite structures and (b) suggested CO_2 adsorption mechanism on Na-zeolite.

became smaller. The IR band that appeared at 2347 cm^{-1} can be assigned in two ways: O=C=O linearly adsorbed on Na^+ ions less exposed than those originating band at 2355 cm^{-1} [39] and weaker interaction of CO_2 with Na^+ ion when two CO_2 molecules share the same Na^+ site [42]. The latter is more plausible given the previous discussion of CO_2 adsorption due to the increased affinity between Na^+ ions and CO_2 molecules inside the small pores. Either way, the observed peak at 2347 cm^{-1} resulted from the direct interaction of CO_2 with Na^+ ions. These results indicate that CO_2 primarily adsorbs on the induced dipoles of Na-zeolites and/or direct interaction with Na^+ ions.

Interestingly, unlike the other three Na-zeolites, a distinct IR peak was observed in Na-ZSM-5 at around 1639 cm^{-1}, which can come from carbonate-like species (CO_3^{2-}) [43]. For this type of carbonate to be formed by CO_2 adsorption on a Na-zeolite adsorbent, it is typically possible at an acid-basic site in the zeolite framework induced by Na^+ ion exchange (Scheme 1b) [44]. Since Na^+ has a lower charge density than H^+, when exchanged in the extraframework of aluminosilicate zeolite, the zeolite framework can have a Lewis acidic property relatively weaker than H^+. The electron density of Na^+ bonded framework oxygen generated by the substation of aluminum atoms becomes relatively higher than the case for H^+, and thus, the Lewis basic sites can also be generated. As a result, a pair of acid-basic sites can be formed near the Na^+-exchanged site. In general, the acid sites of zeolites can be analyzed using amine-based molecules, such as NH_3 as a probe molecule. Comparing the NH_3-TPD profiles of H-zeolites and Na-zeolites, the former had a strong acid site over 400 °C, while this strong acid site disappeared and the intermediate acid sites at around 300 °C were more prominent in the Na-zeolites (Fig. S9). This trend was evident in ZSM-5.

In addition, the in-situ IR analysis using pyridine molecules as a probe molecule can distinguish the two different acid sites, i.e., Brønsted and Lewis acids [45,46]. When comparing the py-IR data of four Na-zeolites, the Lewis acid site was much more prominent than the Brønsted acid for all the four zeolites (Fig. S10 and Table S1). Furthermore, the smallest pore Na-ZSM-5 still maintained a strong IR band even at high temperatures, indicating the relatively strong Lewis acid property. From the previous CO_2-TPD analysis (Fig. 1d), it was confirmed that Na-ZSM-5 has the strongest CO_2 adsorption site, i.e., the strongest basic site, among the prepared Na-zeolites. Therefore, Na-ZSM-5 possesses a relatively strong Lewis acid-basic site compared to the other four Na-zeolites, and thus this strong adsorption site makes carbonate formation possible. As shown in Fig. 3b, the characteristic IR peak for carbonate species was still observed even at 70 °C. This also serves as one of the contributing factors to the high CO_2 adsorption capacity of low silica Na-ZSM-5 adsorbent.

3.4. Practical aspect of Na-ZSM-5 adsorbent for DAC system

Here, we focused on Na-ZSM-5 with the lowest Si/Al ratio of 11.5 among the zeolites prepared for application in the DAC system since it exhibited the best CO_2 adsorption performance in this study (Fig. 2b). The purpose of DAC technology is to capture CO_2 from the atmosphere. For the development of such a system, the long-term durability of the adsorbent is a critical factor. According to this, we assessed the durability of Na-ZSM-5 through 20 cyclic tests under the low concentration of CO_2 (400 ppm in He balance). As shown in Fig. 4a, despite the slight performance variations from cycle to cycle, no significant degradation was observed throughout the cycles. Notably, this low silica Na-ZSM-5 maintained a high CO_2 adsorption performance with an average CO_2 capacity of ca. 0.35 mmol g^{-1}. This result also presented that the temperature of 300 °C for desorption is sufficient for Na-ZSM-5 to be active for CO_2 adsorption without the pretreatment at 450 °C. The superior long-term stability and the high capacity offer a significant advantage from a practical application perspective.

As the system we want to apply is direct air capture, we further evaluated the CO_2 adsorption performance of atmospheric air over the low silica Na-ZSM-5 using a packed-bed reactor. Dry and wet conditions refer to the flow of 530 ppm CO_2 with an N_2 balance and the atmospheric air with humidity, respectively. Similar to the previous findings, Na-ZSM-5 exhibited a superior CO_2 capacity compared to the corresponding H-ZSM-5. As shown in Fig. 4b, H-ZSM-5 exhibited an exceptionally low CO_2 adsorption capacity of 0.02 mmol g^{-1}, regardless of dry and wet conditions. In contrast, Na-ZSM-5 showed a much higher CO_2 adsorption capacity of 0.26 mmol g^{-1} under the dry condition, and it decreased by ca. 23 % in the wet condition. In the packed-bed system to measure CO_2 adsorption using a gas cell equipped with FT-IR, differences in balance gas, sample form, and gas hourly space velocity existed compared to the previous CO_2 breakthrough curve experiment with TCD. These system differences resulted in a lower CO_2 adsorption capacity of 0.26 mmol g^{-1} compared to 0.35 mmol g^{-1}, despite using the same Na-ZSM-5 (11.5). In addition, we confirmed that the captured CO_2 in the sample was fully desorbed during the desorption process, regardless of the feeding environment, dry or wet conditions. In addition, the CO_2 capture profile over Na-ZSM-5 as a function of time on stream followed a typical Gaussian distribution, and the adsorption was maintained for about 500 sec under the wet condition (Fig. 4c). These results demonstrate that the low silica Na-ZSM-5 is also effective for adsorbing CO_2 even in atmospheric air containing oxygen and moisture. Furthermore, when comparing the CO_2 adsorption capacity of Na-ZSM-5 with those of other adsorbents reported in the literature, the low silica

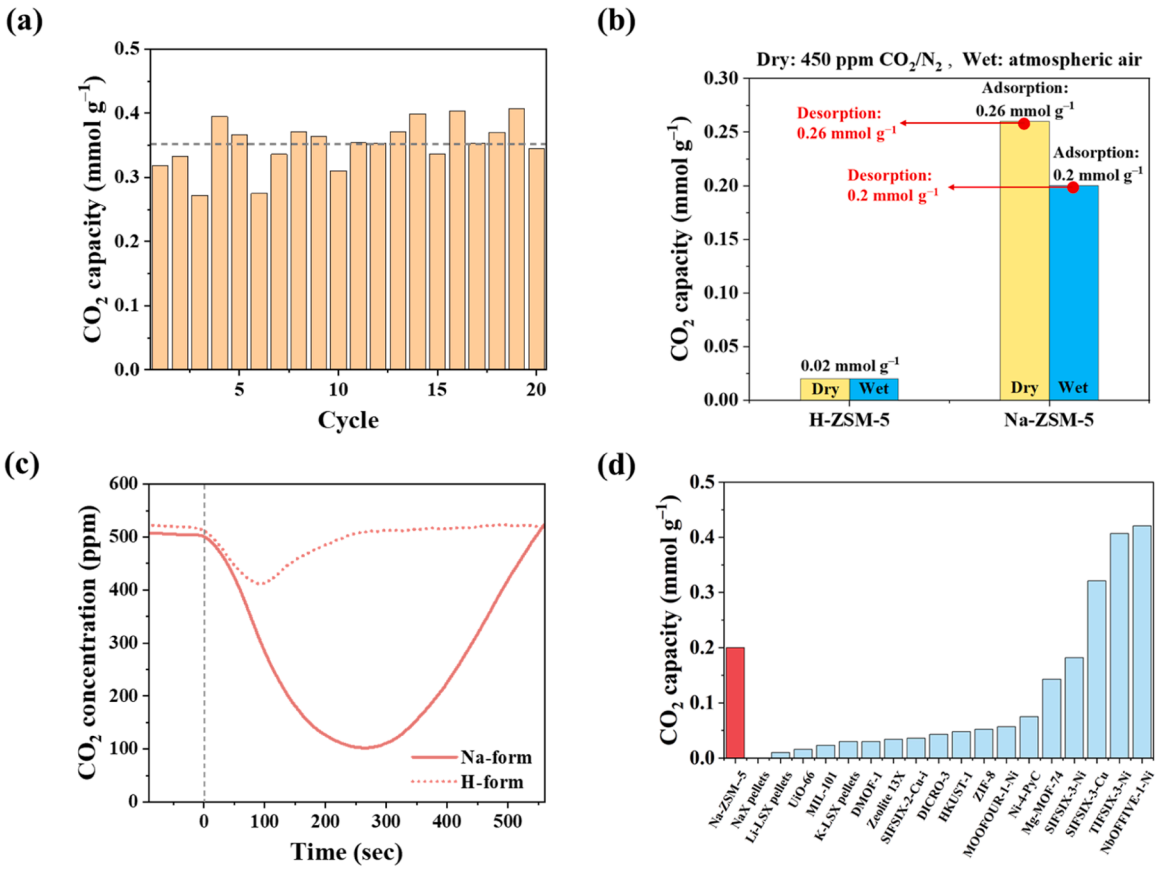

Fig. 4. Practical CO_2 capture properties of Na-ZSM-5 (Si/Al = 11.5). (a) Long-term durability test through 20 times repetitive adsorption-desorption cycles with 400 ppm CO_2. (b) Comparison of CO_2 capacities for adsorption and desorption under dry and atmospheric wet conditions and (c) CO_2 capture profile as a function of time under an atmospheric wet condition in DAC system. For comparison, the data for H-ZSM-5 were added. (d) Comparison of CO_2 capacities under wet condition between Na-ZSM-5 and the other state-of-the-art adsorbents reported in literature. Their test details are noted in Table S2.

Na-ZSM-5 surpassed the average reported values (Fig. 4d and Table S2). Considering its simple formulation and easy accessibility, different from other complex adsorbents, we can suggest the potential for this commercial zeolite as a sorbent for DAC.

The in-situ DRIFTS experiments were also conducted to examine the CO_2 adsorption-desorption behavior under the practical application condition. Fig. 5a presents the IR spectrum obtained from the low silica Na-ZSM-5 exposed to the CO_2/N_2 flow at 25 °C for 30 min. Similar to the previous DRIFTS characterization results (Fig. 3a), the IR peak corresponding to O=C=O linearly adsorbed on Na^+ was mainly observed at 2355 cm^{-1} (Scheme 1b). The IR peaks for carbonate species were also observed at 1624 and 1678 cm^{-1}. These did not completely disappear even when the measuring temperature increased to 250 °C (Fig. 5b). This is in good agreement with the CO_2-TPD result of Na-ZSM-5 with Si/Al = 11.5, which has the strongest basic site (Fig. 2d). Interestingly, when the DRIFTS experiment was performed under the condition of an additional supply of 21 % O_2 to make a similar atmospheric condition, almost identical IR bands were observed but with much higher intensity (Figs. 5c, d). The CO_2 adsorption capacity was also increased to 0.32 mmol g^{-1}. These results indicate the increased CO_2 capture performance in the presence of O_2. Additionally, the carbonate formation is more pronounced in the presence of O_2, thus further enhancing CO_2 chemisorption and overall capture performance.

Fig. 5e illustrates the in-situ DRIFT spectra of Na-ZSM-5 exposed to atmospheric air containing moisture and oxygen. While the characteristic IR peaks similar to the DRIFTS results under the dry condition described above were observed at the initial measurement (5 min), the intensity of the strongest peak appeared at 2355 cm^{-1} decreased gradually with the passage of time (10 min), and a new peak appeared at 2349 cm^{-1} at the same time. This newly observed peak corresponds to the asymmetric stretching mode of free gas CO_2 molecule [47]. This phenomenon can be explained by the competitive adsorption between CO_2 and H_2O, i.e., although atmospheric CO_2 is initially adsorbed through interaction with abundant Na^+, after some time, CO_2 is desorbed due to the competitive adsorption of H_2O. On the other hand, the intensity of the carbonate peak did not decrease with time but increased and was even more pronounced than those measured under dry conditions. These results indicate that the main adsorption mechanism of CO_2 in atmospheric conditions is carbonate form at the acid-basic site in Na-ZSM-5 (Scheme 1b). As shown in Fig. 5f, the carbonate formed in this way was still strongly adsorbed even when the temperature increased to 250 °C as shown in the inert gas flow conditions (Figs. 5b,d).

4. Conclusions

In this study, the adsorption-desorption characteristics of low concentration CO_2 in an atmospheric level were systematically investigated over the H- and Na-forms of commercial zeolites (ZSM-5, Mordenite, Beta and Y) with similar Si/Al ratios. Among the prepared zeolite adsorbents, Na-ZSM-5 exhibited a suitable DAC performance owing to its relatively smaller pore size and stronger acid-basic property. The CO_2 adsorption capacity of Na-ZSM-5 was more pronounced at lower Si/Al ratios due to the abundant adsorption sites derived from more Na^+ ions. The low silica Na-ZSM-5 maintained its CO_2 adsorption capacity even after multiple adsorption-desorption cycles, indicating its durability for practical applications. Based on these results, the low silica Na-ZSM-5 was applied to the DAC system and found to effectively adsorb CO_2 through its strong acid-basic site, mainly as a carbonate form on the site,

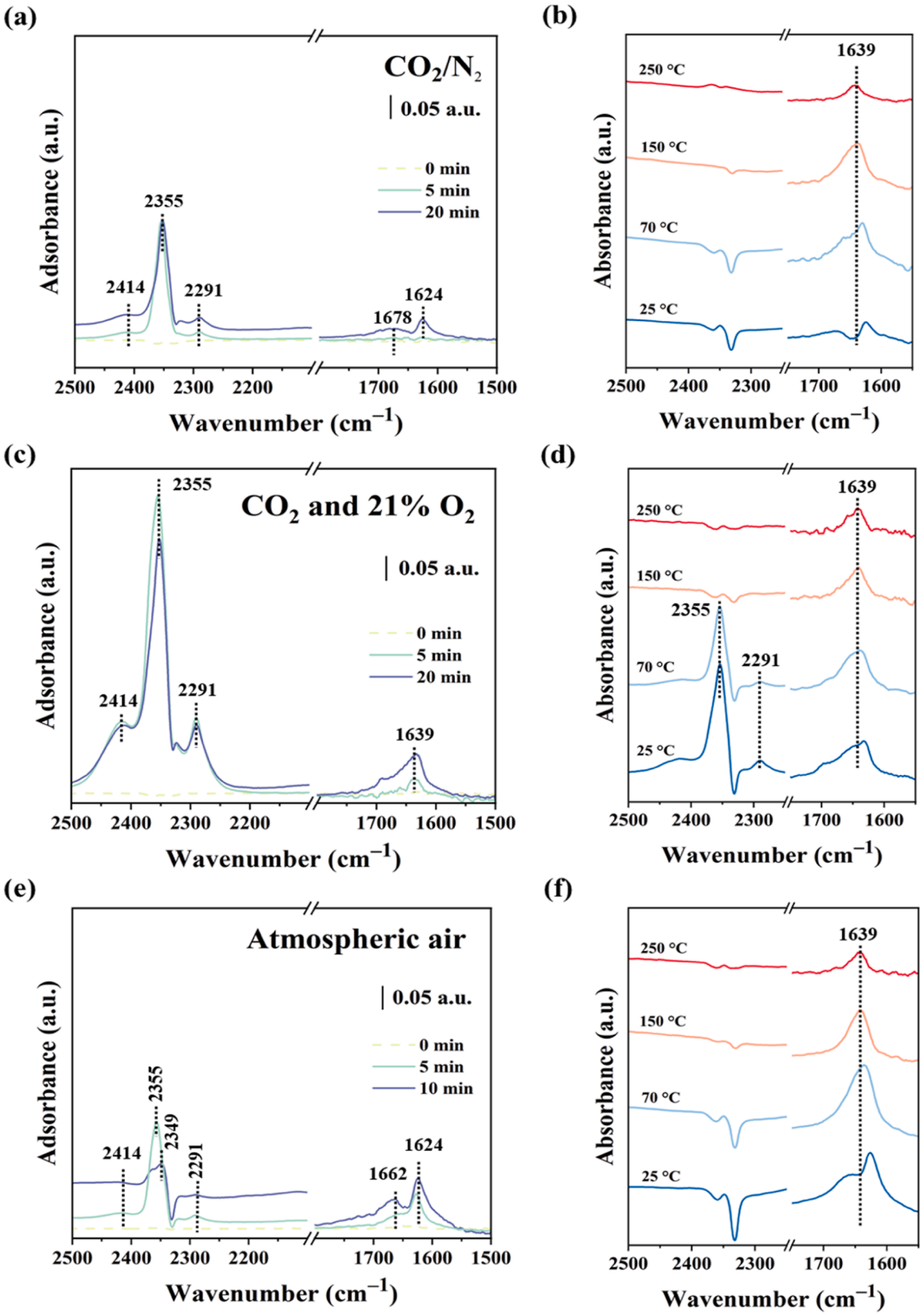

Fig. 5. Adsorbed species in CO_2 adsorption-desorption over Na-ZSM-5 (Si/Al = 11.5). DRIFT spectra measured at 25 °C under the flow of (a) CO_2 in N_2 balance, (c) CO_2 and 21 % O_2 in N_2 balance, and (e) atmospheric air, and (b, d, and f) each IR spectrum obtained during consecutive CO_2 desorption in N_2 flow at a temperature range of 25 to 250 °C.

despite the presence of oxygen and moisture. These findings emphasize the importance of zeolite adsorbents with medium pore size, low Si/Al ratio and robust acid-basic sites as promising candidates for the DAC system that offers a potential net-zero solution.

CRediT authorship contribution statement

Do Yeong Kim: Writing – original draft, Methodology, Investigation, Formal analysis, Data curation, Conceptualization. **Wo Bin Bae:** Investigation, Formal analysis, Data curation. **Haehyun Min:** Formal analysis, Data curation. **Kyeong-Hun Ryu:** Formal analysis, Data curation. **Sungjoon Kweon:** Formal analysis, Data curation. **Linh Mai Tran:** Formal analysis, Data curation. **Young Jin Kim:** Investigation, Formal analysis, Data curation. **Min Bum Park:** Writing – original draft, Supervision, Investigation, Funding acquisition, Formal analysis. **Sung Bong Kang:** Writing – original draft, Supervision, Investigation, Funding acquisition, Formal analysis, Conceptualization.

Declaration of competing interest

The authors declare that they have no known competing financial interests or personal relationships that could have appeared to influence the work reported in this paper.

Acknowledgements

This study was supported by the National Research Foundation of Korea (NRF) Grant funded by the Korean government (MSIT) (No. 2021R1C1C1005404 and 2021R1A5A1028138) and Korea Institute of Marine Science & Technology Promotion (KIMST) funded by the Ministry of Oceans and Fisheries (2520000248).

Supplementary materials

Supplementary material associated with this article can be found, in the online version, at doi:10.1016/j.apsadv.2024.100664.

Data availability

Data will be made available on request.

References

[1] W. Yu, T. Wang, A.-H.A. Park, M. Fang, Review of liquid nano-absorbents for enhanced CO_2 capture, Nanoscale 11 (2019) 17137–17156, https://doi.org/10.1039/C9NR05089B.
[2] A. Samanta, A. Zhao, G.K. Shimizu, P. Sarkar, R. Gupta, Post-combustion CO_2 capture using solid sorbents: a review, Ind. Eng. Chem. Res. 51 (2012) 1438–1463, https://doi.org/10.1021/ie200686q.
[3] C. Chen, S. Zhang, K.H. Row, W.-S. Ahn, Amine–silica composites for CO_2 capture: a short review, J. Energy Chem. 26 (2017) 868–880, https://doi.org/10.1016/j.jechem.2017.07.001.
[4] Y. Belmabkhout, V. Guillerm, M. Eddaoudi, Low concentration CO_2 capture using physical adsorbents: Are metal–organic frameworks becoming the new benchmark materials? Chem. Eng. J. 296 (2016) 386–397, https://doi.org/10.1016/j.cej.2016.03.124.
[5] A.E. Ogungbenro, D.V. Quang, K. Al-Ali, M.R. Abu-Zahra, Activated carbon from date seeds for CO_2 capture applications, Energy Procedia 114 (2017) 2313–2321, https://doi.org/10.1016/j.egypro.2017.03.1370.
[6] E. Sanz-Pérez, A. Arencibia, G. Calleja, R. Sanz, Tuning the textural properties of HMS mesoporous silica. Functionalization towards CO_2 adsorption, Micropor. Mesopor. Mat. 260 (2018) 235–244, https://doi.org/10.1016/j.micromeso.2017.10.038.
[7] Y. Kong, Y. Zhong, X. Shen, S. Cui, M. Yang, K. Teng, J. Zhang, Facile synthesis of resorcinol–formaldehyde/silica composite aerogels and their transformation to monolithic carbon/silica and carbon/silicon carbide composite aerogels, J. non-cryst. solids 358 (2012) 3150–3155, https://doi.org/10.1016/j.jnoncrysol.2012.08.029.
[8] C. Chen, W.-S. Ahn, CO_2 capture using mesoporous alumina prepared by a sol–gel process, Chem. Eng. J. 166 (2011) 646–651, https://doi.org/10.1016/j.cej.2010.11.038.
[9] U.H. Bhatti, D. Sivanesan, D.H. Lim, S.C. Nam, S. Park, I.H. Baek, Metal oxide catalyst-aided solvent regeneration: A promising method to economize post-combustion CO_2 capture process, J. Taiwan Inst. Chem. Eng. 93 (2018) 150–157, https://doi.org/10.1016/j.jtice.2018.05.029.
[10] S. Yaqub, L.S. Pei, N. Mellon, A.M. Shariff, Performance evaluation of covalent organic polymer adsorbent prepared via microwave technique for CO_2 and CH_4 adsorption, Procedia Eng. 148 (2016) 249–253, https://doi.org/10.1016/j.proeng.2016.06.604.
[11] C. Xu, G. Yu, J. Yuan, M. Strřmme, N. Hedin, Microporous organic polymers as CO_2 adsorbents: advances and challenges, Mater. Today Adv. 6 (2020) 100052–100060, https://doi.org/10.1016/j.mtadv.2019.100052.
[12] B. Dutcher, M. Fan, A.G. Russell, Amine-based CO_2 capture technology development from the beginning of 2013- A Review, ACS Appl. Mater. Interfaces 7 (2015) 2137–2148, https://doi.org/10.1021/am507465f.
[13] C. Xu, N. Hedin, Microporous adsorbents for CO_2 capture–a case for microporous polymers? Mater. Today 17 (2014) 397–403, https://doi.org/10.1016/j.mattod.2014.05.007.
[14] G. Martra, R. Ocule, L. Marchese, G. Centi, S. Coluccia, Alkali and alkaline-earth exchanged faujasites: strength of Lewis base and acid centres and cation site occupancy in Na-and BaY and Na-and BaX zeolites, Catal. Today 73 (2002) 83–93, https://doi.org/10.1016/S0920-5861(01)00521-1.
[15] W.H. Chan, M.N. Mazlee, Z.A. Ahmad, M.A.M. Ishak, J.B. Shamsul, The development of low cost adsorbents from clay and waste materials: a review, J. Mater. Cycles Waste Manag. 19 (2017) 1–14, https://doi.org/10.1007/s10163-015-0396-5.
[16] S. Kulprathipanja, Zeolites in Industrial Separation and Catalysis, John Wiley & Sons, 2010.
[17] S.M. Wilson, The potential of direct air capture using adsorbents in cold climates, iScience 25 (2022) 105564–105584, https://doi.org/10.1016/j.isci.2022.105564.
[18] D. Fu, M.E. Davis, Toward the feasible direct air capture of carbon dioxide with molecular sieves by water management, Cell Rep. Phys. Sic. 4 (2023) 101389–101402, https://doi.org/10.1016/j.xcrp.2023.101389.
[19] M. Song, G. Rim, F. Kong, P. Priyadarshini, C. Rosu, R.P. Lively, C.W. Jones, Cold-temperature capture of carbon dioxide with water coproduction from air using commercial zeolites, Ind. Eng. Chem. Res. 61 (2022) 13624–13634, https://doi.org/10.1021/acs.iecr.2c02041.
[20] D. Fu, Y. Park, M.E. Davis, Zinc containing small-pore zeolites for capture of low concentration carbon dioxide, Angew. Chem. 61 (2022) e202112916, https://doi.org/10.1002/anie.202112916.
[21] K.S. Kencana, S.B. Hong, Nanocrystalline sodium mordenite as an efficient low-concentration CO_2 adsorbent, Sep. Purif. Technol. 350 (2024) 128018–128024, https://doi.org/10.1016/j.seppur.2024.128018.
[22] D. Fu, Y. Park, M.E. Davis, Confinement effects facilitate low-concentration carbon dioxide capture with zeolites, PNAS 119 (2022) e2211544119, https://doi.org/10.1073/pnas.2211544119.
[23] Z. Tao, Y. Tian, S.Y. Ou, Q. Gu, J. Shang, Direct air capture of CO_2 by metal cation-exchanged LTA zeolites: Effect of the charge-to-size ratio of cations, AIChE J. 69 (2023) e18139, https://doi.org/10.1002/aic.18139.
[24] D. Fu, M.E. Davis, Carbon dioxide capture with zeotype materials, Chem. Soc. Rev. 51 (2022) 9340–9370, https://doi.org/10.1039/D2CS00508E.
[25] C. Emeis, Determination of integrated molar extinction coefficients for infrared absorption bands of pyridine adsorbed on solid acid catalysts, J. Catal. 141 (1993) 347–354, https://doi.org/10.1006/jcat.1993.1145.
[26] C. Zhang, H. Yang, P. Gao, H. Zhu, L. Zhong, H. Wang, W. Wei, Y. Sun, Preparation and CO_2 hydrogenation catalytic properties of alumina microsphere supported Cu-based catalyst by deposition-precipitation method, J. CO2 Util. 17 (2017) 263–272, https://doi.org/10.1016/j.jcou.2016.11.015.
[27] M. Miyamoto, Y. Fujioka, K. Yogo, Pure silica CHA type zeolite for CO_2 separation using pressure swing adsorption at high pressure, J. Mat. Chem. 22 (2012) 20186–20189, https://doi.org/10.1039/C2JM34597H.
[28] D.P. Serrano, R.A. Garcia, M. Linares, B. Gil, Influence of the calcination treatment on the catalytic properties of hierarchical ZSM-5, Catal. Today 179 (2012) 91–101, https://doi.org/10.1016/j.cattod.2011.06.029.
[29] M. Rasouli, N. Yaghobi, S. Chitsazan, M.H. Sayyar, Influence of monovalent cations ion-exchange on zeolite ZSM-5 in separation of para-xylene from xylene mixture, Micropor. Mesopor. Mat. 150 (2012) 47–54, https://doi.org/10.1016/j.micromeso.2011.09.013.
[30] D. Barthomeuf, Framework induced basicity in zeolites, Micropor. Mesopor. Mat. 66 (2003) 1–14, https://doi.org/10.1016/j.micromeso.2003.08.006.
[31] R.V. Siriwardane, M.-S. Shen, E.P. Fisher, J. Losch, Adsorption of CO_2 on zeolites at moderate temperatures, Energy & Fuels 19 (2005) 1153–1159, https://doi.org/10.1021/ef040059h.
[32] J. Zhang, R. Singh, P.A. Webley, Alkali and alkaline-earth cation exchanged chabazite zeolites for adsorption based CO_2 capture, Micropor. Mesopor. Mat. 111 (2008) 478–487, https://doi.org/10.1016/j.micromeso.2007.08.022.
[33] M. Zhang, W. Qian, H. Ma, W. Ying, H. Zhang, P. Yuan, Molecular insights into adsorption and diffusion properties of CO_2/CH_4 in cation-exchanged ZSM-5 zeolites, J. Phys. Chem. C 128 (2024) 6962–6970, https://doi.org/10.1021/acs.jpcc.4c01027.
[34] S. Storck, H. Bretinger, W.F. Maier, Characterization of micro- and mesoporous solids by physisorption methods and pore-size analysis, Appl. Catal. A Gen. 174 (1998) 137–146, https://doi.org/10.1016/S0926-860X(98)00164-1.
[35] C. Chen, W.-S. Ahn, CO_2 adsorption on LTA zeolites: Effect of mesoporosity, Appl. Surf. Sci. 311 (2014) 107–109, https://doi.org/10.1016/j.apsusc.2014.04.218.
[36] B. Beagley, J. Dwyer, F. Fitch, R. Mann, J. Walters, Aluminum distribution and properties of faujasites. Basis of models and zeolite acidity, J. Phys. Chem. 88 (1984) 1744–1751, https://doi.org/10.1021/j150653a017.

[37] T. Ohgushi, Y. Kawanabe, Properties of Na ions in NaZSM-5 zeolite, Zeolites 14 (1994) 356–359, https://doi.org/10.1016/0144-2449(94)90109-0.
[38] R. Osuga, T. Yokoi, J.N. Kondo, Probing the basicity of lattice oxygen on H-form zeolites using CO_2, J. Catal. 371 (2019) 291–297, https://doi.org/10.1016/j.jcat.2019.02.003.
[39] B. Bonelli, B. Civalleri, B. Fubini, P. Ugliengo, C.O. Areán, E. Garrone, Experimental and quantum chemical studies on the adsorption of carbon dioxide on alkali-metal-exchanged ZSM-5 zeolites, J. Phys. Chem. B 104 (2000) 10978–10988, https://doi.org/10.1021/jp000555g.
[40] B. Bonelli, B. Onida, B. Fubini, C.O. Areán, E. Garrone, Vibrational and thermodynamic study of the adsorption of carbon dioxide on the zeolite Na−ZSM-5, Langmuir 16 (2000) 4976–4983, https://doi.org/10.1021/la991363j.
[41] A. Pulido, M. Delgado, O. Bludský, M. Rubeš, P. Nachtigall, C.O. Areán, Combined DFT/CC and IR spectroscopic studies on carbon dioxide adsorption on the zeolite H-FER, Energy Environ. Sci. 2 (2009) 1187–1195, https://doi.org/10.1039/B911253G.
[42] K. Hadjiivanov, H. Knözinger, FTIR study of the low-temperature adsorption and co-adsorption of CO and N_2 on NaY zeolite: evidence of simultaneous coordination of two molecules to one Na^+ site, Chem. Phys. Lett. 303 (1999) 513–520, https://doi.org/10.1016/S0009-2614(99)00229-8.
[43] S. Coluccia, L. Marchese, G. Martra, Characterisation of microporous and mesoporous materials by the adsorption of molecular probes: FTIR and UV–Vis studies, Micropor. Mesopor. Mat. 30 (1999) 43–56, https://doi.org/10.1016/S1387-1811(99)00019-0.
[44] G. Busca, Acidity and basicity of zeolites: A fundamental approach, Micropor. Mesopor. Mat. 254 (2017) 3–16, https://doi.org/10.1016/j.micromeso.2017.04.007.
[45] T.K. Phung, M.M. Carnasciali, E. Finocchio, G. Busca, Catalytic conversion of ethyl acetate over faujasite zeolites, Appl. Catal. A 470 (2014) 72–80, https://doi.org/10.1016/j.apcata.2013.10.028.
[46] R. Ferwerda, J.H. van der Maas, P.J. Hendra, Pyridine adsorbed on Na-faujasite: a FT-Raman spectroscopic study, J. Phys. Chem. 97 (1993) 7331–7336, https://doi.org/10.1021/j100130a035.
[47] G. Herzberg, Molecular Spectra and Molecular Structure, van Nostrand Reinhold, New York, 1950.